JOURNAL OF MATERIALS SCIENCE 22 (1987) 1087–1096

Study of the correlation between hardness and structure of nitrogen-implanted titanium surfaces

J. C. PIVIN, F. PONS, J. TAKADOUM
Centre de Spectrométrie Nucléaire et de Spectrométrie de Masse, BP 1, 91406 Orsay, France
H. M. POLLOCK
Department of Physics, University of Lancaster, Lancaster LA1 4YB, UK
G. FARGES
Etablissement Technique Central de l'Armement (E.T.C.A.), 16 Bis Avenue Prieur de la Code d'Or, 94114 Arcveil, France

Several spectroscopies analysing the composition and chemical nature of thin films (Rutherford backscattering spectrometry, nuclear reaction analysis, secondary ion mass spectroscopy, X-ray photoelectron spectroscopy) were combined with a specially designed technique of X-ray diffraction at grazing incidence on bulk samples, in order to characterize $Ti_{1-x}N_x$ films of nearly homogeneous composition obtained by ion implantation at several energies. Differences in the nature of the phases observed, with respect to previous TEM studies on thin foils, are discussed in terms of radiation-enhanced diffusion and of thermal dissipation of the ion-beam power. The distribution of nitrogen atoms, defects and phases as a function of the nitrogen concentration are also correlated with changes in depth profiles of hardness measured by a submicroscopic indentation test.

1. Introduction

The advantages offered by ion implantation or ion mixing compared with other surface treatments in specific cases of protection against friction and wear are now well documented [1, 2]. Ion implantation is particularly promising when surface finish must be preserved and the material is to be protected by a hard but ductile and adherent film in not too severe conditions of abrasion. This is the reason for important research dealing with nitrogen or carbon implantation in ferrous alloys used as tools for the cutting and forming of softer materials.

Compared with the case of steels, few studies have been performed on the tribological behaviour of another important technological alloy, Ti6Al4V, implanted with nitrogen [3–10]. The wear improvement was correlated with the hardening of superficial layers by δ-TiN precipitates (with a close packed orientation relationship of the fcc precipitates and cph α-Ti matrix) and by compressive elastic stress in the residual α-$Ti_{1-x}N_x$ matrix (lattice expansion) [4]. The development of tensile stress in less implanted regions to balance the compression at intermediate depths was also observed in these TEM experiments; it may contribute to the increase in surface hardness. The latter was estimated to be a factor of 2 for a Ti–60%N film 50 nm thick resulting from the implantation of 45 keV N^+ ions, by a submicroscopic indentation test [10]. In another TEM study [9] it was shown that the initial composition of the δ-nitride precipitates is $Ti–N_{0.5}$, and that they grow and their stoichiometry increases by radiation-enhanced diffusion of the nitrogen atoms. However, they finally attain a maximum size and stoichiometry ($TiN_{1.1}$) and, because of the local stress in the matrix, their density is limited. Precipitates of another, less stable hardening phase, ε–Ti_2N, were then observed at higher implantation doses. The maximum density of precipitates and the threshold of concentration at which they appear seems to depend upon the ion-beam current which affects both density of mobile defects and temperature.

A reduction of the friction coefficient was only observed when an amorphous TiO film containing hard TiN precipitates, or grown upon a hard α-Ti + δ-TiN sublayer, was formed during nitrogen implantation [5–8]; this film was produced either by recoil-implantation of the contamination layer or by direct oxidation during high-temperature implantation. Such a behaviour is analogous to the resistance to seizure of other amorphous films formed during friction of titanium or iron alloys lubricated with thiophosphate or molybdenum sulphide [11, 12], and also of amorphous NiB, NiP films produced by boron or phosphorus implantation into nickel [13]. It has been proposed that the hard α-Ti + δ-TiN layer might stabilize the lubricating amorphous layer of TiO or $TiO_{1-x}N_x$ [5]. An application is expected in the field of protheses [6, 14] since titanium alloys or TiN coatings exhibit too high a friction coefficient and would induce inflammation of joints (in such

0022–2461/87 $03.00 + .12

TABLE I Theoretical parameters of implantation

Energy (keV)	Mean projected range of ions, R_p(nm)			Standard deviation, ΔR_p (nm)			Mean projected range of defects, R_d (nm)		Sputtering yield (Ti atoms/ion)
	WSS	TRIM	COSIPO	WSS	TRIM	COSIPO	TRIM	COSIPO	
190	345	361	350	102	86	137	323	315	0.23
100	185	197	200	71	58	87	163	165	0.34
30	55	63	67	31	23	40	34	40	0.60
190 + 100 + 30*	245	250		230	230		180		

*Given values are for the sum distribution with implanted doses in the ratio 1, 0.69, 0.30.

applications the opposing surface is generally a softer plastic).

Note also that little is known of the intrinsic properties of physical (PVD) or chemical vapour deposited (CVD) TiN coatings, because they exhibit stoichiometry gradients and various textures according to the deposition process used [15]. Hardnesses between 1100 and 3000 kg mm^{-2} have been reported [10, 15, 16] and it is thought that ε-Ti_2N coatings formed under lower nitrogen pressures (or as sub-layers during δ-TiN deposition) are intrinsically harder. Thus pure, homogeneous and isotropic films formed by ion implantation of nitrogen into pure titanium would paradoxically help us to understand the properties of thicker coatings. However, only one study has dealt with the wear behaviour of pure titanium implanted with nitrogen (without observed oxygen contamination and in the absence of the hardening δ-phase of the TA6V alloy) [17], and the respective contributions of nitrogen, oxygen or carbon to the protection of titanium alloy surfaces by Ti–O–C–N amorphous layers need to be analysed.

The first results of such a study are reported here. Single-phased and pure α-$Ti_{1-x}N_x$, ε-Ti_2N_x or δ-TiN_x films were obtained by implanting pure titanium with well-filtered N^+ ion beams of successively decreasing energies. Such conditions of implantation should allow us to obtain films of homogeneous composition over a large range of depths if implanted atoms would remain statistically distributed as predicted by the theory; but their diffusion during the cascades alters the depth distribution. However, the absolute composition of the films was determined by Rutherford backscattering spectrometry (RBS) and nuclear reaction analysis (NRA) and depth profiles were obtained by secondary ion mass spectrometry (SIMS). The structure of films was established by grazing incidence X-ray diffraction (with a depth resolution of 50 nm) and by X-ray photoelectron spectroscopy (XPS) of the electronic structure. A submicroscopic indentation experiment was used to measure the hardness of films. It has been shown elsewhere that the intrinsic hardness of films as thin as 50 nm can be measured by this technique, providing that the indentation depth is measured continuously during loading and unloading, and then corrected from the elastic recovery in the depth of the imprint [18]. The correlation between hardness and structure of the films is discussed.

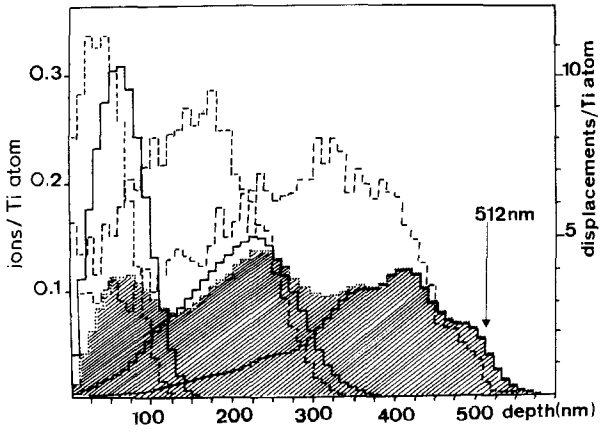

Figure 1 Theoretical distributions of (——) implanted ions and (– – –) damage calculated by the TRIM computer simulation program, with 1000 ions impinging upon the titanium target at each energy of 190, 100 and 30 keV. The dashed profile is the sum of distributions obtained for implanted doses in the ratios, 1, 0.6, 0.3 at 190, 100 and 30 keV respectively.

2. Implantations and dosages of implanted films

2.1. Implantations

The samples were cut from pure titanium rod provided by Material Research S.A. (Marz quality with a total impurity content less than 10^{-3}, essentially 5 to 8 $\times$ 10^{-4} O, 1 to 2 $\times$ 10^{-4} C). Their surfaces were polished with diamond pastes down to a 0.01 μm average roughness, then implanted in the C.S.N.S.M. machine [19] under a vacuum better than 10^{-7} torr. The energies of the $^{14}N^+$ ions implanted were chosen on the basis of the W.S.S. tables [20] and of the TRIM program [21, 22]; they were also compared to values calculated by Keinonen [23] and Hautala [24] with the computer simulation program for polycrystals (COSIPO) (Table I – the coefficient of inelastic energy loss is uncertain for light ions of energies over 10 keV/nuclei, and only the COSIPO attempts to take into account the widening of implantation profiles due to the channelling of ions). The ion doses implanted successively at energies of 190, 100 and 30 keV were set in the ratio 1, 0.69, 0.30, respectively, to try to obtain a homogeneous nitrogen concentration profile in the implanted layer over a depth of 500 nm.

Fig. 1 shows the theoretical distribution of implanted ions for low nominal concentrations. The actual distribution was expected to be flatter, because of the commonly observed smearing out of elemental distributions implanted at a single energy into metals [25, 26]. It is quite impossible to calculate a profile

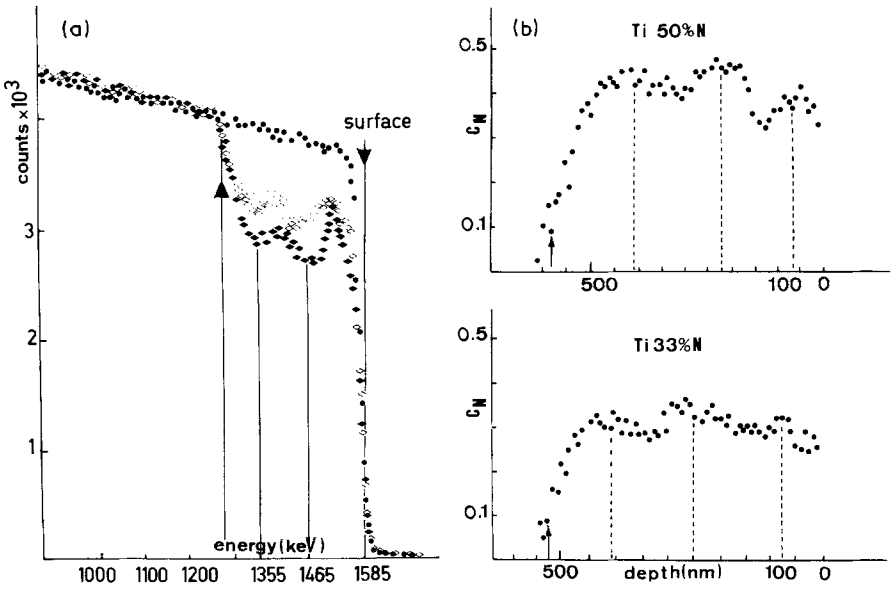

Figure 2 RBS analysis with He^+ ions of 2.0 MeV of implanted titanium (●) and titanium implanted with nominal concentrations of 33% N (◇), 50% N (◆): (a) raw energy distribution of ions backscattered by titanium atoms at an angle of 165°; (b) nitrogen profile deduced by an iterative calculation program of inelastic energy losses in the target before and after the scattering event.

for high concentrations (over ~10% N) because the target stopping power changes continuously with composition, then with depth and with the course of implantation. Moreover, the direction of the nitrogen diffusion enhanced by radiation damages is expected to change with the implanted dose [26], since interstitial sinks are the surface and less implanted regions at low doses, while they are the already formed precipitates at high doses [4, 9].

2.2. Concentration measurements and depth profiles by RBS and NRA

The real in-depth distributions of nitrogen atoms could not be determined by RBS for all implanted doses, since a light species in a heavier matrix is detected with difficulty by this technique. For nominal concentrations higher than 10%, they were deduced from Rutherford backscattering spectra of the in-depth distribution of host metal atoms (Fig. 2), obtained with a 2 MeV $^4He^+$ beam delivered by the Van de Graaff accelerator of the Ecole Normale Superieure, Paris. The depth resolution of these profiles is of about 15 nm and the uncertainty on concentrations (due to statistical fluctuations in counts) is of 1% N.

The total amounts of ^{14}N, ^{12}C and ^{16}O in these samples and in an unimplanted titanium surface was also measured by NRA, using the $^{14}N(d,p)^{15}N$ and the $^{12}C(d,p)^{13}C$, $^{16}O(d,p)^{17}O$ reactions with deuterons of 1.6 and 0.8 MeV, respectively. The total numbers of nitrogen, carbon, oxygen and titanium atoms per cm^2 (measured by RBS for titanium) are given in Table II. One can see that the surfaces are slightly contaminated with oxygen (and carbon to a lesser extent) after implantation, despite the fact that the ion current was always kept below 5 $\mu A\,cm^{-2}$ in order to avoid substantial heating of the sample during implantation. However, titanium surfaces react strongly with oxygen, carbon and nitrogen, and atoms of the contamination layer which are recoil-implanted by the N^+ ions or sputtered, are continuously replaced by CO molecules of the residual gas. Moreover, titanium atoms can diffuse during collision cascades and contribute to the oxide growth; the energy distribution of emitted protons indicates indeed that the contamination remains very superficial. A maximum thickness of the oxide film was calculated by assuming it was a pure TiO_2 rutile one (Table II): it is higher for Ti–34% N than for Ti–50% N, maybe because of sputtering and

TABLE II Measured doses and concentrations

Nominal nitrogen dose (10^{15} atom/cm^2)	Measured total amounts in the film (10^{15} atom/cm^2)				Mean nitrogen stoichiometry	TiO_2 thickness (nm)
	N	O	C	Ti(*)		
0	10 ± 2	38 ± 12	10 ± 2	2645 ± 10		6 ± 2
46	63	16	5	2664	$Ti_{0.98}N_{0.02}$	3
282	279	30	5	2515	$Ti_{0.90}N_{0.10}$	5
554	579	62	7	2403	$Ti_{0.81}N_{0.19}$	10
720	730	70	16	2317	$Ti_{0.76}N_{0.24}$	11
930	1050	110	20	2159	$Ti_{0.67}N_{0.33}$	17
1380	1593	48	8	2027	$Ti_{0.56}N_{0.44}$	8

*The number of titanium atoms was summed until a depth containing less than 15% of the implanted concentration (marked by an arrow in Fig. 2) and it was then diminished of the number of titanium atoms contained in the oxide film. It corresponds to a thickness of 470 nm in the case of the unimplanted surface and of 570 nm for Ti–50% N.

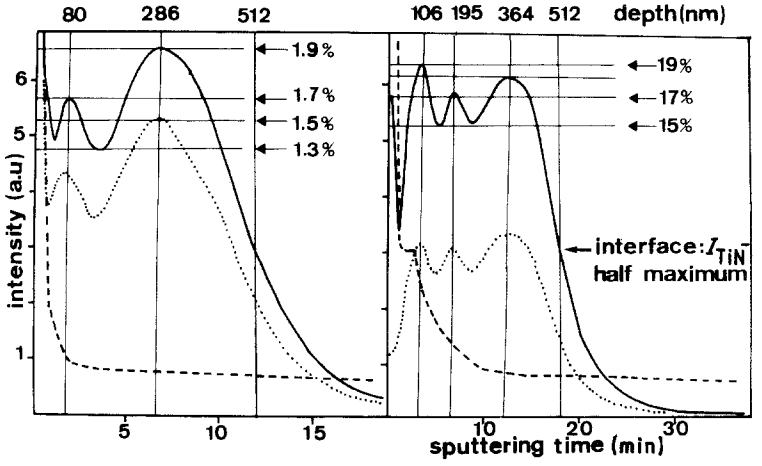

Figure 3 SIMS analysis with Cs^+ ions of 10 keV of titanium surfaces implanted with nominal concentrations of 2% N (left) and 20% N (right): ——$^{62}TiN^-$ secondary ions, ...$^{110}Ti_2N^-$, – – –$^{16}O^-$ or $^{12}C^-$; the intensities of these last species is greater than 100 on the same scale in the contamination layer. The arrows show the mean concentration measured by RBS in the first 150 nm of the films, and deduced values of the concentration extremes.

slight differences in sample heating. These quantitative analyses also show that the actual implanted doses of nitrogen are somewhat higher than the nominal ones, because one cannot prevent part of the secondary electrons emitted in the ion implanter optics under N^+ bombardment from giving an electron current which is directly subtracted from the integrated ion current. These electrons are repelled onto the surface by the grids used to repel those emitted by the target itself.

2.3. SIMS profiles of the depth distribution of nitrogen, carbon and oxygen in implanted films

The high sensitivity and the somewhat better depth resolution of this technique permitted us to determine the nitrogen, carbon and oxygen profiles with a better accuracy. The machine used was a CAMECA 3F ion microscope; details of its optics are given by Slodzian [27]. The primary ions were Cs^+ of energy 10 keV, with a mean projected range of 2.7 nm at an angle of incidence of 30° with respect to the surface. Such a bombardment causes much damage in the outermost layers (2 displacements per atom for each incident ion) and thus gives a high value of the sputtering yield. Sputtering rates of 1450 and 1700 nm h^{-1} were measured on Ti_2N and TiN PVD coatings under our experimental conditions by means of crater profilometry. These were compared to the sputtering rates of implanted films; the interface marked by an arrow on profiles of Fig. 3 is inferred to be at the same depth for all concentrations, namely that measured by RBS for the higher concentrations (500 to 525 nm). The values are in good agreement for nitrogen contents over 10% and thus the depth scales of profiles are approximately linear.

Secondary ions TiN^- and Ti_2N^- were selected in the mass spectrum as the best to characterize the nitrogen distribution, because few N^- ions are emitted, and other polyatomic emissions overlap with various more intense $Ti_xO_yC_z^-$ emissions. The profiles of Fig. 3 show clearly that the nitrogen depth-distribution is different for surfaces implanted with low concentrations (2% and 10% nominal values) and for nominal concentrations over 20%. In the first case, it exhibits maxima at depths corresponding approximately to the theoretical sum-profile (of Fig. 1), while in the second case maxima of concentration correspond rather to the elemental profiles of ions implanted at each of the energies 30, 100 and 190 keV. This effect will be discussed later.

Table III gives the nominal concentrations, the mean concentration measured by RBS, and the depth positions of the extremes measured by RBS and by SIMS. Nitrogen concentrations at the extremes were calculated by calibrating the mean intensity of the first TiN^- peak on the mean concentration measured by RBS over this range of depth. It was also assumed that the emission yield of TiN^- ions does not vary if the variations of concentration are no more than 20% of their mean values. The in-depth position and concentrations of extremes measured by SIMS are approximately equal to those measured by RBS for the highest implanted doses.

The depth profiles of $^{16}O^-$ and $^{12}C^-$ ions exhibit a bump at an approximate depth of 60 nm corresponding about to the range of recoil atoms with a maximum transferred energy by 30 keV N^+ ions. However, the intensity of this bump is always less than 1% of the level in the contamination layer, in agreement with the results of NRA.

3. Structure of the films

3.1. X-ray diffraction at grazing incidence

The specially designed goniometer and detector are described in another paper [28]. The incidence angle, α, of a monochromatic X-ray beam at the surface of a bulk sample can be set to a value very near the angle of specular reflection (α_c = 0.30 to 0.33° for $Ti_{1-x}N_x$ alloys), and then increased step by step in order that increasing thicknesses of the sample will contribute to diffraction. This thickness, z, is related to the absorption coefficient, μ, of X-rays in the material studied, to the angle of diffraction, 2θ, and to the chosen contribution, y, of deeper layers to the yield of diffraction, according to the formula:

$$z = \frac{\ln(1/y)}{\mu(1/\sin\alpha) + 1/\sin(2\theta - \alpha)}$$

For instance z is of 90 to 150 nm, for $\alpha = \alpha_c$, $\theta = 20°$ and $y = 5\%$ in the studied $Ti_{1-x}N_x$ alloys.

A complete diffractogram is registered for each value of z, then the contribution of slices of equal thicknesses Δz to a given diffraction peak are derived. This requires an X-ray beam of high intensity, which

TABLE III Nitrogen concentration extremes

Nominal concentrations (%)	Mean nitrogen concentration (%)		Depth of maxima (nm)		Nitrogen concentration extremes (%)			
					RBS		SIMS	
	20–470 nm	40–60 nm	RBS	SIMS	max	min	max	min
1.7	1.7	1.5		80			1.7	1.3
				285			1.9	
10.3	10.0	8.5		95			10	7.5
				290			11	
20.3	19.4	17	80	105	20	15	19	15
			230	195	25	17	17	16
			350	360	20		18	
26.4	24.0	20	55	55	26	18	22	18
			230	150	28	22	28	21
			360	360	24		22	
34.1	32.7	29	80	75	32	30	39	35
			250	240	37	30	37	31
			410	385	39		33	
50.5	44.0	40	60	65	40	35	47	35
			230	220	45	40	47	38
			405	410	44		44	

was in the present study the synchrotron radiation of the L.U.R.E. in Orsay (filtered by a rotating curved monochromator to give a chosen incident beam wavelength between 0.09 and 0.21 nm).

Figs 4 and 5 show, for instance, partial diffractograms over an angular interval 2θ from 34 to 46°, recorded at increasing depths of 160, 380, 600 and 900 nm for two nominal concentrations of 20 and 50% N. It is clear that only the nitride ε-Ti_2N is formed in the first case, while the δ-TiN phase is observed in outermost layers and ε-Ti_{2N} at intermediate depths (ca. 350 to 550 nm) in the second case.

For nominal contents of 2% and 10% N only the solid solution α-$Ti_{1-x}N_x$ is identified. Its measured parameter indicates that the lattice swelling remains less than 0.5%. However, the multiplication of planar defects and local strains induce a widening of diffraction peaks. For films of nominal concentrations 20% and 26% N, the measured intensity of α-$Ti_{1-x}N_x$ peaks on the outermost 350 nm decreases then falls to zero (or at least is too small to measure); ε-Ti_2N becomes the main constituent of these outer layers Fig. 6. At these depths δ-TiN appears in the film implanted with 34% N, and is the only phase identified in that implanted with 50% N (Fig. 6).

This analysis is confirmed by the uniqueness of the

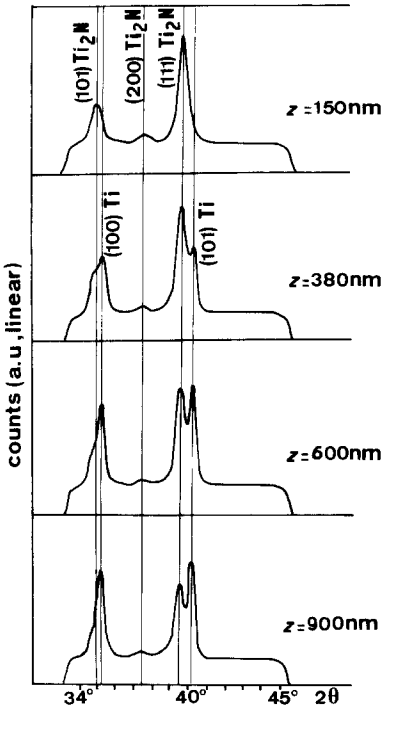

Figure 4 Partial diffractograms of implanted layers recorded with 0.150 nm X-rays at incidence angles of 0.50, 1.30, 1.80, 2.30° on Ti–20% N.

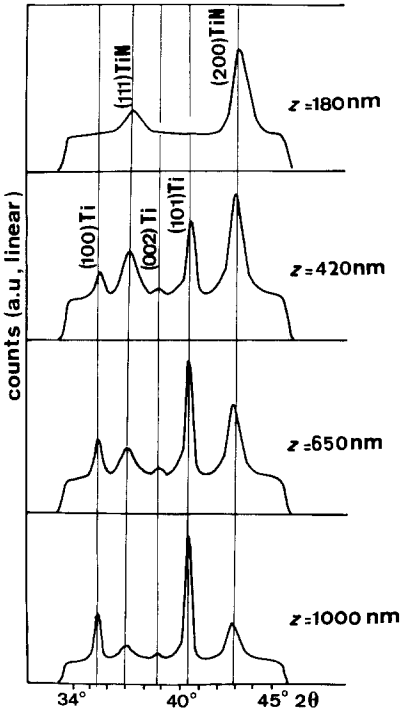

Figure 5 Partial diffractograms recorded under the same conditions as in Fig. 4 on Ti–50% N.

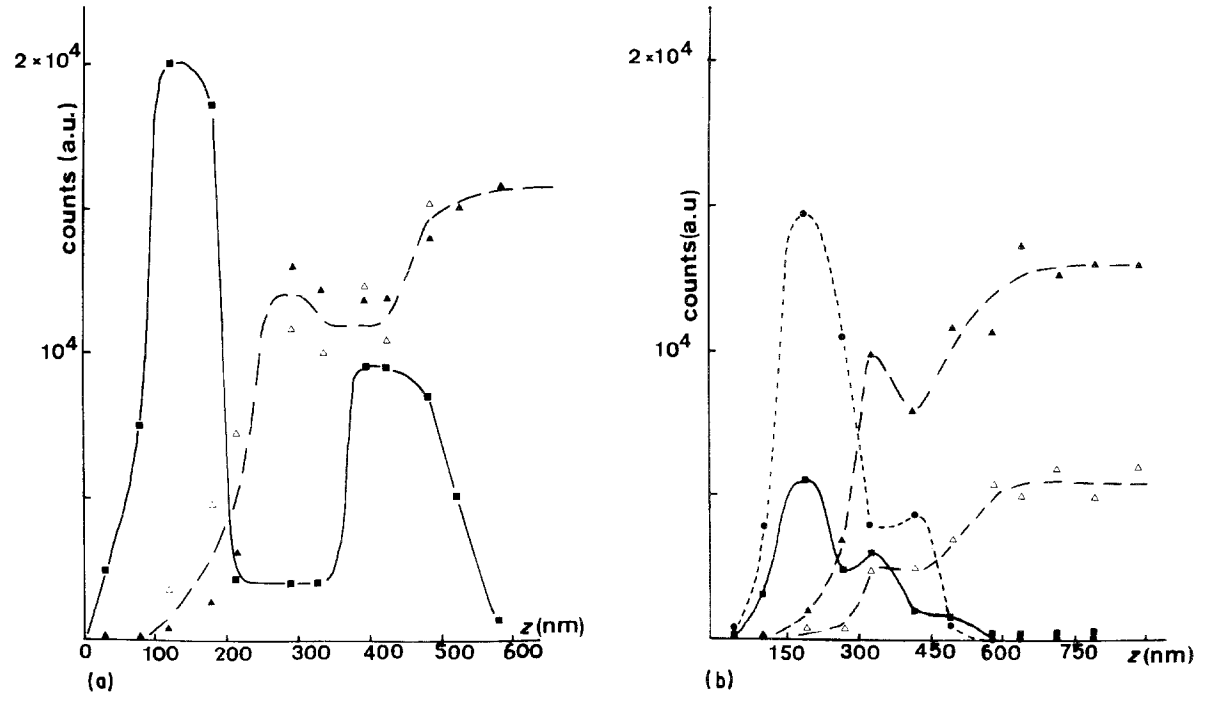

Figure 6 Variations of the concentration of each phase in slices of thickness $\Delta z = 50$ nm, as a function of depth z, deduced from measurements of peak intensities. (a) (■) (1 1 1) Ti_2N, (△) (1 0 0) Ti, (▲) (1 0 1) Ti. (b) (●) (2 0 0) TiN, (■) (1 1 1) TiN, (▲) (1 0 1) Ti, (△) (1 0 0) Ti.

binding energy of each electronic level measured at a depth of 40 to 70 nm, after removal of the contamination layers by ion bombardment.

3.2. XPS analysis of the electronic structure

The instrument used was a Leybold LHS10 spectrometer described by Poloschegg [29] and Wechsung [30]. The spectra were recorded with an Al$K\alpha$ radiation and with a constant spectrometer pass-energy (constant interval of kinetic energy of collected electrons), equal to 50 eV. The energy scale was calibrated, and the work function of the analyser was determined, by assessing the measured binding energy of the lines Au 4f7/2 and Cu 2p3/2, their now well accepted values being, respectively, (84 00 ± 0.04) eV and (932.70 ± 0.02) eV [31]. The energy resolution of all spectra can be estimated as 0.4 to 0.5 eV on the basis of the measured FWHM of the Au 4f7/2 peak which was 1.2 eV for a natural width of 0.8 eV.

The residual pressure in the target chamber was always better than 2×10^{-9} torr, and surfaces were sputtered by Ar^+ ions of relatively low energy (1500 eV) at an incidence angle of 45°. The mean range of defects induced by Ar^+ ions at this energy is much less than the thickness analysed by XPS (escape depth of about 2 nm for Ti2p, Nls and valence band electrons with kinetic energies over 1000 eV) and the stoichiometry of the layers analysed does not seem to have been altered too much by this cleaning procedure. Indeed, neither splitting of the core level emissions into a nitride and a metal peak (as commonly observed in surfaces depleted in light carbon, nitrogen or oxygen atoms by an ionic bombardment [32], nor widening of the peaks was noticed. Here the difference of binding energies between titanium and TiN is three times the resolution of the spectrometer; splitting of peaks separated by 0.5 eV with other materials could easily be observed under the same analytical conditions. Moreover, a linear relationship was established between the intensity of the N1s emission and the nitrogen content measured by RBS, both for the whole range of concentration of implanted films and for Ti_2N and TiN PVD coatings also studied (with deviations of less than $\Delta I = 1\%$ from the line $I/(I)_{TiN} = C_N/(C_N)_{TiN}$). The thickness of material sputtered by Ar^+ ions before analysis was estimated to be 40 nm, and concentrations of films analysed by XPS are given in the third column of Table III.

Fig. 7 shows the Ti 2p1/2 and Ti 2p3/2 levels for four concentrations of implanted films. Note that if the surface was contaminated with oxygen, TiO_2 peaks would appear at 459.0 and 464.8 eV (for Ti2p3/2 and 2p1/2 levels, respectively). A continuous shift in energy of each level with the nitrogen concentration is observed, but without broadening due to the overlap of emissions by two phases: half the FWHM of the 2p3/2 peak is in all cases 1.1 eV, which is less than the difference of binding energy in titanium and TiN (see Fig. 8). Similarly, no broadening is observed for the N1s level (half FWHM 1.0 eV) and the peak is symmetrical. However, the shift in energy of this peak is less than the Ti2p one, and it corresponds to the shift of the Fermi level, ε_F; the latter was located at half the height of the Ti3d band (see Fig. 9). This lower shift can be explained by the fact that nitrogen atoms have in all cases titanium neighbours, and that the screening function of core levels is mainly affected by the nearest neighbours. Note that a similar shift of ε_F has been observed in CVD TiN coatings with increasing stoichiometries [33].

The assessment of peaks in the valence band (Fig. 9) was made on the basis of its previous analysis for CVD TiN coatings or single crystals [33, 36] and APW calculations [36, 37]. The interesting fact which can be

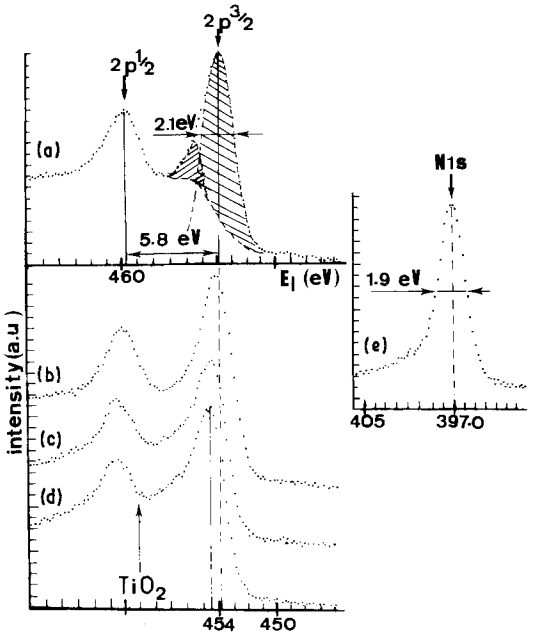

Figure 7 X-ray photoelectron spectra of the Ti 2p core level recorded with an Al$K\alpha$ radiation on (a) unimplanted titanium, (b) Ti–10% N, (c) Ti–33% N, (d) Ti–50% N. The dotted curves plotted on the (a) spectrum show the procedure used for the background subtraction and the decomposition of the Ti 2p3/2 peak into a principal peak and its satellite. Horizontal arrows show the FWHM of the Ti 2p3/2 peak. (e) N1s core level recorded on Ti–50% N.

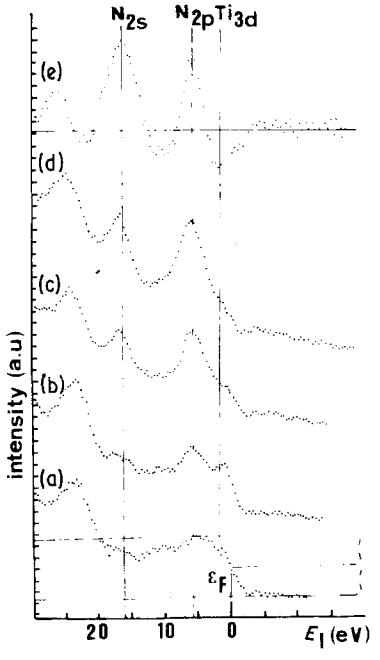

Figure 9 X-ray photoelectron spectra of the valence band recorded for (a) unimplanted titanium, (b) Ti–10% N, (c), Ti–34% N, (d), Ti–50% N, (e) subtraction of (a) from (d) showing evidence for the contribution of N 2s and N 2p hybridized levels to the band. The peak at 25 eV is the Ti 3d emission excited by the unfiltered Al$K\alpha$ 3,4 satellite radiation.

noted concerning the changes in the valence band with the stoichiometry of films is that the overlap between the Ti3d and N2p levels (σ bonds between hybridized orbitals 3d Eg and 2sp) is stronger than the overlap between the Ti 3d and N2s levels (π bonds); a total of one electron is transferred from each titanium to nitrogen atoms in stoichiometric TiN. As the ratio C_N/C_{Ti} increases, the intensity of the Ti3d band decreases linearly, but the ratio of the intensities of the N2s and N2p band does not remain constant. A linear increase of this ratio due to the difference in the overlap with Ti3d is observed, as noted previously for CVD coatings (Fig. 10). Note that the decrease in the intensity of Ti3d (despite its crude estimation) corresponds to the loss of one 3d electron in the Ti–50% N implanted film or in the TiN PVD coating studied, as against two electrons in pure titanium. This linear relationship also supports the uniqueness of the structure.

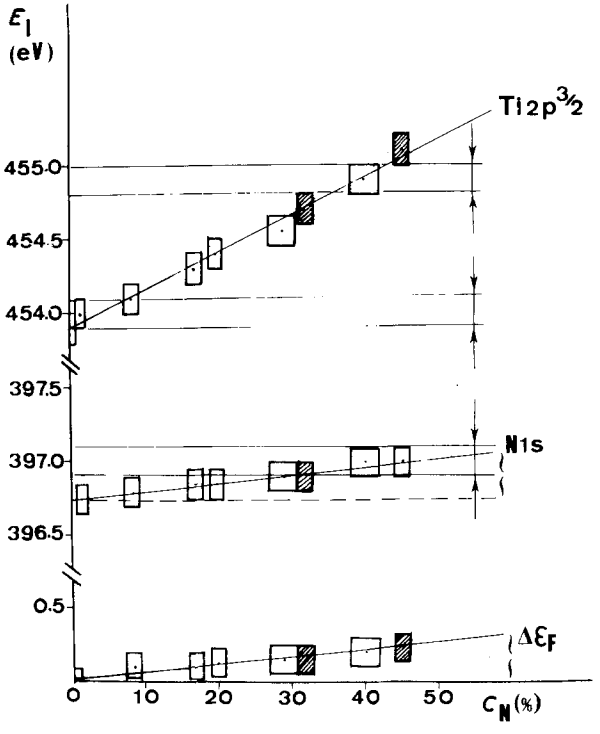

Figure 8 Measured shift in energy of the Ti 2p3/2, N 1s core levels and of the Fermi level, ε_F, as a function of the nitrogen concentration measured by RBS, in implanted films (□) and in two ε-Ti_2N, δ-TiN PVD coatings (▨). The size of squares corresponds to the uncertainty in the binding energy and concentration. Arrows show the binding energies measured by other authors on TiN CVD coatings and on pure titanium (33, 34, 35).

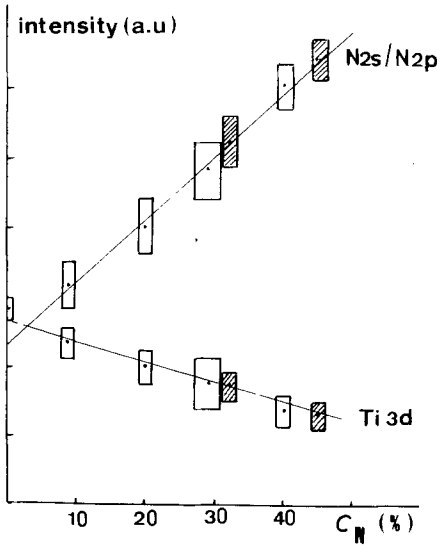

Figure 10 Intensities of the Ti 3d unbinding level, T_2G, and of the N 2s/N 2p ratio as a function of C_N (same comments as for Fig. 8).

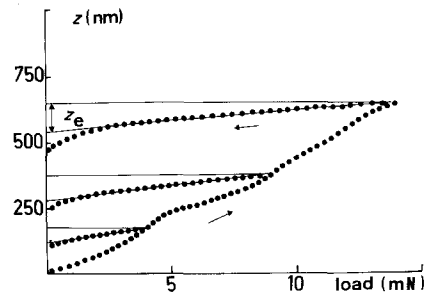

Figure 11 Some raw indentation loading (→) and unloading (←) curves with different maximum loads recorded on Ti–50% N.

4. Hardness measurements

More details on the technique and on limits to the measurement of the intrinsic hardness of films thinner than a micrometer can be found in Ross *et al.* [18] and Pollock *et al.* [38]. The depth of indentation, z, by a trigonal (very sharp cutting) diamond is continuously recorded during loading and unloading. From a series of recordings on each sample are derived:

1. The elastic recovery in the depth of the imprint, z_e, (the recovery in the diagonal is taken into account) during unloading. Its relative amount, $R = z_e/z$, is inversely proportional to $E/H(1 - \nu^2)$, where H is the mean pressure of indentation (or hardness), ν the Poisson ratio and E is Youngs elastic modulus.

2. The hysteresis area, W, between loading and unloading curves. If the indented solid is fully rigid plastic and has a yield strength independent of depth, the plot of $W^{2/3}$ as a function of the load, F, is a straight line, whose slope raised to the power -3, is a plasticity index equal to $9KH$ (K is a geometrical constant of the diamond).

3. The plastic indentation depth (or off-load depth), $z_p = z(1 - R)$, which varies as the square root of the load in the simple case mentioned above for W. The slope, raised to the power -2, is another plasticity index, I_p, equal to KH.

Fig. 11 shows some of the raw curves for the film implanted with 50% N, and Figs 12 and 13 the variations of z_e, z_p and $W^{2/3}$ with F, for the two highest concentrations and for pure titanium. For other hard implanted films on a soft substrate previously studied with this technique [18], the elastic recovery exceeds that of titanium even at loads for which the substrate is penetrated: R is effectively constant ($25 \pm 1\%$) until $z_p = 500$ nm for 34 and 50% N instead of 5% for

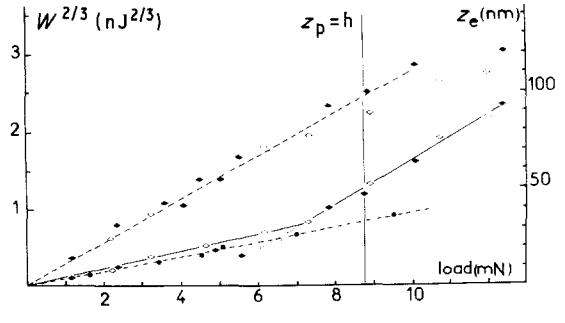

Figure 12 (——) $W^{2/3}$ and (– – –) z_e as a function of load, F, for: (●) unimplanted titanium, (◇) titanium implanted with 34% N, (◆) titanium implanted with 50% N.

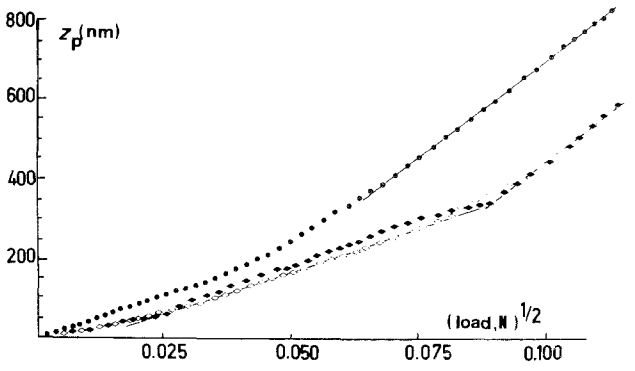

Figure 13 Plastic indentation depth as a function of $(F)^{1/2}$ for the same films as in Fig. 12.

pure titanium (thus I_p/R and hence E will vary as I_p over the whole implanted thickness). On the other hand, the curves $z_p = f(F)^{1/2}$ and $W^{2/3} = f(F)$ exhibit a change of slope for a load of about 7.3 mN, corresponding to a real penetration of implanted layers, z_p, of (350 ± 20) nm, ~ 0.7 times the film thickness. Note that a factor of 0.8 was also found in the case of Ni–B implanted films on to nickel with comparable hardness of films and substrate [18].

A faint shoulder is also observed in the $W^{2/3}$ curve of the Ti–50% N film at a load near 5.6 mN ($z_p = \sim 240$ nm), which reflects that of the raw loading curves.

For all the films studied, and even for pure titanium, a change of slope is also observed on the $W^{2/3}$ and z_p curves at a critical load which depends on the film hardness: 2.5 mN for titanium and 1.25 mN for Ti–34% N or Ti–50% N. It is certainly due in part to the work hardening by polishing before indentation (especially for pure titanium and low nitrogen contents), and in part to the contribution of the unavoidable contamination film to measurements at shallow depths. In the case of the hardest films (for which radiation damage and nitride hardening dominates over work hardening) this change of slope occurs at depths lower than 70 nm, as for hard NiB films: this seems to be the minimum film thickness for which the intrinsic hardness can be measured with our technique.

Note also that the plasticity index F/z_p^2 and F^3/W^2 measured on the part of the curves intrinsic to the TiN films are always in the ratio (9 ± 0.5), which fact helps to confirm the validity of the results.

In order to analyse the influence of the nitrogen implantation upon the matrix hardness independently of the work hardening, the plasticity index, $I_p = F/z_p^2$, was normalized to the pure titanium value at each depth. The corresponding increase in off-load hardness is plotted as a function of the real penetration in the implanted film, z_p, in Fig. 14. The agreement between the variations of hardness as a function of depth and nominal nitrogen content, and the variations of nitrogen concentration profiles or phase concentration profiles is astonishingly good, as is discussed below (despite the change in thickness of contamination films, but the apparent hardening at depths lower than 70 nm for all the films studied is perhaps due to the finite radius of the curvature of the diamond tip, and thus is corrected by our normalization).

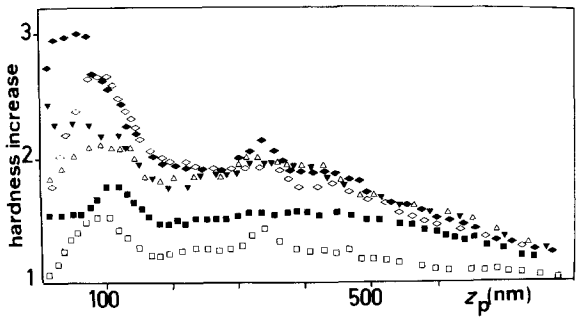

Figure 14 Factor of hardness increase with respect to pure titanium as a function of the plastic indentation depth: (□) Ti–2% N; (■) Ti–10% N; (△) Ti–20% N; (▼) Ti–25% N; (◇) Ti–33% N; (◆) Ti–50% N.

5. Discussion and conclusions

Let us first compare the absolute hardness of pure titanium, measured by means of a Vickers test with indentation depths between 1 and 10 μm (well over the work-hardened thickness), with that of implanted films and of the TiN PVD coating studied, as deduced from their plasticity index normalized to titanium. The hardness of titanium being (2.5 $\pm$ 0.1) GPa and its plasticity index (20 $\pm$ 1) GPa (at large depths where it is not work hardened), the hardness of the outer layer of δ-TiN formed on the Ti–50% N and Ti–34% N implantation films is (17.5 $\pm$ 1.5) GPa. For the δ-TiN PVD coating a constant hardness of (52.5 $\pm$ 2.5) GPa was measured for indentation depths of between 25 and 200 nm, and a value of (40 $\pm$ 5) GPa for indentation depths of between 300 and 1000 nm by means of a Vickers test (this is a crude estimation because Vickers hardness tests were performed on thicknesses for which the result must be considered with caution, since the coating was only 5.7 μm thick). Taking this into account, the two values are in good agreement, but very much higher than reported values of the hardness of bulk TiN (17 to 23 GPa according to the author) [10, 38, 39] or those of various CVD coatings of δ-TiN or ε-Ti_2N (ranging between 12 and 27 GPa) [15]; but often the latter type of measurement is made by means of a Vickers test on thicknesses for which the substrate alters the result, and a wide range of structures and crystallographic textures is involved. The PVD coating studied here had a columnar structure with a diameter of columns of about 1 μm and a marked fibre texture [1 1 1]. On the other hand, implanted films are formed of submicroscopic grains with isotropic orientations. These preliminary remarks illustrate the relativity of the concept of hardness, which depends on the scale at which it is measured with respect to the size of mobile defects. Values of the Youngs modulus were also derived from H/R, equal to 110 GPa for titanium, 65 GPa for the Ti–50% N film and 490 GPa for the δ-TiN coating; in the two first cases these values are very close to those measured by tensile tests, namely 120 for titanium and 78 to 84 for TiN [39, 40].

The observed modifications of nitrogen profiles and distribution of phases with the nitrogen content can easily be understood in terms of enhanced diffusion of nitrogen atoms by radiation damage at room temperature, already noticed by several authors for nitrogen in titanium alloys or steels [9, 23, 24]. At low implanted concentrations it contributes only to a widening of the sum-profile, while at high implanted concentrations it contributes to the growth and increase of stoichiometry of the already formed precipitates which are sinks for the nitrogen atoms (strain in the matrix is thus reduced). The ions being successively implanted at three energies, the nitrogen concentration profile tends to peak at the mean range of ions for each energy.

Now the differences in the nitrogen profiles and in the order of formation of phases with respect to other studies can be due to differences of sample heating. In the present study, the phases appear in the order of increasing nitrogen content in the diagram, as generally is the case when they form and grow only by radiation-enhanced diffusion of defects created during the collision cascades [26]. On the other hand, the formation of the δ-TiN phase before ε-Ti_2N in other studies on TA6V [4–9] seems to indicate a substantial heating of the target (the samples were often thin films for electron microscopy and the dissipation of energy in such cases is often difficult). Indeed the most stable δ-TiN phase cannot form without displacement of atoms on large distances. A difference in depth distribution of nitrogen and a preferential formation of δ-TiN was also observed by Keinonen in a recent study [23]; but the implantation current was ten times that used in the present experiments, and complicated changes in the nitrogen distribution were attributed to a blistering of nitrogen. The observation in the present study of a maximum in the distribution of the nitrides at an intermediate depth near 100 nm, followed by their expansion towards the surface, is consistent with the fact that nitrogen atoms will migrate towards the surface only when the stoichiometry of the formed nitride has attained its upper value at the mean range of the ions.

Now as the concentration is varied, the changes in the depth profile of hardness and in its maximum value account for the expected effects of the creation of damage (2% N), hardening by solute nitrogen atoms in α-Ti (10% N), formation (20% N) then expansion (26% N) of Ti_2N, and finally formation (34% N) then expansion (50% N) of TiN. Indeed the hardness exhibits alternatively a maximum at a depth near 100 nm (for 2%, 20%, 34% N) or near the surface (for 10%, 26%, 50% N), corresponding to the distributions of nitrogen and of the nitride phases in the first 200 to 300 nm of the surface. The hardness level off at depths of between 200 and 400 nm corresponds rather to the more oblate peak of the nitrogen sum-profile (at a depth near 290 nm for 2%, 10% N) or of the deeper elemental profile (at a depth near 400 nm for 20% to 50% N); the phases observed at these depths are also a mixture of nitrides and α-Ti. Note also that the hardness measured for Ti–34% N and Ti–50% N in the same range of depths, where inverse gradients of the δ-TiN and ε-Ti_2N concentrations were revealed by X-ray diffraction experiments, is close to the hardness of the pure Ti_2N film formed for lower nitrogen concentrations.

In conclusion, the present study shows the interest

of combining several analyses of the composition and structure, in order to elucidate the intricate effects of changes in concentration and diffusion enhanced by radiation damages on the crystallographic nature and hardness of phases formed in implanted films. The results will allow us to obtain more homogeneous films in further experiments by rectifying the implantation energies and increasing their number. Such films and those of Ti–O–C–N will be characterized in the same way, and then submitted to friction tests. Preliminary experiments of dry friction against steel, and SIMS analysis of the wear tracks, have shown that both the friction and wear resistance are improved by nitrogen implantation [41]. However, for nitrogen concentrations higher than 10%, the nitrides formed are finally pulled away during seizure events; the surface then suffers a more severe oxidizing wear.

Acknowledgements

We thank the Solid State Physic Group of the Ecole Nationale Superieure, Paris, for help with NRA and RBS experiments with the Van de Graaff accelerator. This research was sponsored by the Etablissement Technique Central de l'Armement (ETCA), 16 Bis Avenue Prieur de la Code d'Or, 94114 Arcueil, France.

References

1. I. L. SINGER, *Mat. Res. Soc. Symp. Proc.* **27** (1984) 585.
2. H. HERMAN, Proceedings IBMM (1980), *Nucl. Instrum. Methods* **182–183** (1981) 887.
3. R. G. VARDIMAN, *Mat. Res. Soc. Symp. Proc.* **27** (1984) 699.
4. R. HUTCHINGS, Proceedings SMI2B, *Mat. Sci. Eng.* **69** (1985) 129.
5. R. HUTCHINGS and W. C. OLIVER, *Wear* **92** (1983) 143.
6. R. MARTINELLA, S. GIOVANARDI, G. CHEVALLARD and M. VILLANI, Proceedings SMI2B, *Mat. Sci. Eng.* **69** (1985).
7. D. FLECHE, J. P. GAUTHIER and P. KAPSA, Proceedings Eurotribology 85, Lyon, September 1985, Société Française de Tribologie, Vol. 1 (Elsevier, 1985) 1.4.
8. D. FLECHE, J. P. GAUTHIER, J. PIVOT and J. A. ROGER, *J. Microsc. Spectrosc. Electron.* **10** (1985) 219.
9. K. HOHMUTH and B. RAUSCHENBACK, *Mat. Sci. Eng.* **69** (1985) 489.
10. J. B. PETHICA, R. HUTCHINGS and W. C. OLIVER, *Nucl. Instrum. Methods* **209–210** (1983) 995.
11. E. BELIN, J. L. MANSOT, J. M. MARTIN, H. DEXPERT and P. LAGARDE, Proceedings Eurotribology 85, Lyon, September 1985, Société Française de Tribologie, Vol. 4 (Elsevier 1985) 5.4.
12. J. M. MARTIN, J. L. MANSOT, I. BERBEZIER and H. DEXPERT, *Wear* **93** (1984) 117.
13. J. TAKADOUM, J. C. PIVIN, J. CHAUMONT and C. ROQUES-CARMES, *J. Mater. Sci.* **20** (1985) 1480.
14. *M.R.S. Bull.* November/December (1985) 17.
15. TOSHINORI TAKAGI (ed.), Proceedings International Ion Engineering Congress, Kyoto (1980), several papers by Delera, Matthews, pp. 1313, 1326.
16. G. FARGES, "Caractérisation métallurgique et tribologique des revêtements anti-usure dans le système Ti-N obtenus par PVD ionique", Le Vide, les couches minces, no. spécial "Journées sur les dépots ioniques", Limoges, September (1985), **41** (1986) No. 230, 97.
17. S. R. SHEPARD and N. P. SUH, *J. Lubr. Technol.* **104** (1982) 29.
18. J. ROSS, J. TAKADOUM, H. M. POLLOCK and J. C. PIVIN, *Thin Solid Films*, to be published.
19. J. CHAUMONT, F. LALU, M. SALOMÉ, A. M. LAMOISE and H. BERNAS, *Nucl. Instrum. Methods* **189** (1981) 193.
20. K. B. WINTERBON, "Ion Implantation Range and Energy Deposition Distributions" Vol. 2 (Plenum, New York, 1985).
21. J. P. BIERSACK and L. G. HAZGMARK, *Nucl. Instrum. Methods* **174** (1980) 257.
22. *Idem, ibid.* **182–183** (1981).
23. J. KEINONEN, in Proceedings International Workshop on Solid State Reactions After Ion Implantation Detected by Nuclear Methods, Göttingen (March 1986).
24. M. HAUTALA, *Phys. Rev. B* **30** (1984) 5010.
25. J. TAKADOUM, J. C. PIVIN, J. PONS-CORBEAU, R. BERNERON and J. C. CHARBONNIER, *Surf. Interfac. Anal.* **6** (4) (1984) 174.
26. J. C. PIVIN and J. P. RIVIERE, Proceedings Physics. Congress, Nice (1985), Societé Française de Physique (Les Editions de Physique, Les Illis, France, 1986) 199.
27. G. SLODZIAN, NBS Special Publication 427, Proceedings Workshop on SIMS and IMMA, Gaithersburg (1974) p. 33.
28. F. PONS, M. PEQUIGNOT, J. C. PIVIN, S. MEGTER, D. MAIREY and C. ROQUE-CARMES, *Thin Solid Films*, submitted.
29. H. D. POLOSCHEGG, *Appl. Phys.* **4** (1974) 63.
30. R. WECHSUNG, *Le Vide les couches minces* **38** (1983) 309.
31. M. T. ANTHONY and M. P. SEAH, *Surf. Interfac. Anal.* **6** (3) (1984) 95.
32. J. C. PIVIN, *J. Mater. Sci.* **18** (1983) 1267.
33. L. ROUX, thesis, Aix Marseille II University, September (1981).
34. N. VAN HIEU and D. LICHTMAN, *Appl. Surf. Sci.* **20** (1984) 186.
35. C. D. WAGNER, W. M. RIGGS, L. E. DAVIS, J. F. MOULDER and G. E. MUILENBERG, in "Handbook of X-ray Photoelectron Spectroscopy", (Perkin Elmer, Eden Prairie, Minnesota, 1978).
36. L. I. JOHANSSON, A. CALLENAS, P. M. STEFAN, A. NORLUND CHRISTENSEN and K. SCHWARTZ, *Phys. Rev. B* **24** (1981) 1883.
37. A. NECKEL, P. RASTL, R. EIBLER, P. WEINBERGER, K. SCHWARTZ, *J. Phys.* **C9** (1976) 579.
38. H. M. POLLOCK, D. MAUGIS and H. BARQUINS, in "Microindentation Techniques in Materials Science and Engineering", edited by P. J. Blau and B. R. Lawn (American Society for Testing and Materials, Philadelphia, Pennsylvania, 1986) p. 47.
39. E. A. BRANDES (ed.), "Smithells Metals Reference Book", 6 Ed, (Butterworths, London, 1983) p. 23–1.
40. PASCAL, *Chimie Minérale* **IX.7** (Masson ed. 1963) 135.
41. F. PONS, J. C. PIVIN and G. FARGES, 6th International Conference on Ion Beam Modification of Materials: IBMM 86, Catania, Italy (June 1986), *J. Mat. Research*, submitted.

Received 9 May
and accepted 23 July 1986